Article

Anti-inflammatory and Antiphytopathogenic Fungal Activity of 2,3-*seco*-Tirucallane Triterpenoids Meliadubins A and B from *Melia dubia* Cav. Barks with ChemGPS-NP and In Silico Prediction

Hieu Tran Trung,[||] Kartiko Arif Purnomo,[||] Szu-Yin Yu, Zih-Jie Yang, Hao-Chun Hu, Tsong-Long Hwang, Nguyen Ngoc Tuan, Le Ngoc Tu, Dau Xuan Duc, Le Dang Quang, Anders Backlund, Tran Dinh Thang,* and Fang-Rong Chang*

Read Online

ACCESS | Metrics & More | Article Recommendations | SI Supporting Information

ABSTRACT: Two new rearranged 2,3-*seco*-tirucallane triterpenoids, meliadubins A (**1**) and B (**2**), along with four known compounds, **3**−**6**, were isolated from the barks of *Melia dubia* Cav. Compound **2** exhibited a significant inflammatory inhibition effect toward superoxide anion generation in human neutrophils (EC_{50} at $5.54 \pm 0.36\ \mu M$). It bound to active sites of a human inducible nitric oxide synthase (3E7G) through interactions with the residues of GLU377 and PRO350, which may benefit in reducing the neutrophilic inflammation effect. The ChemGPS-NP interpretation combined with bioactivity assay and in silico prediction results suggested **2** to be an agent for targeting iNOS with different mechanisms as compared to a selected set of current approved drugs. Moreover, compounds **1** and **2** showed remarkable inhibition against the rice pathogenic fungus *Magnaporthe oryzae* in a dose-dependent manner with IC_{50} values of 137.20 ± 9.55 and $182.50 \pm 18.27\ \mu M$, respectively. Both **1** and **2** displayed interactions with the residue of TYR223, a key active site of trihydroxynaphthalene reductase (1YBV). The interpretation of **1** and **2** in the ChemGPS-NP physical-chemical property space indicated that both compounds are quite different compared to all members of a selected set of reference compounds. In light of demonstrated biological activity and in silico prediction experiments, both compounds possibly exhibited activity against phytopathogenic fungi via a novel mode of action.

Meliadubin A (1)   Meliadubin B (2)

Anti-phytopathogenic fungal assays & Anti-inflammatory assays

ChemGPS-NP Web
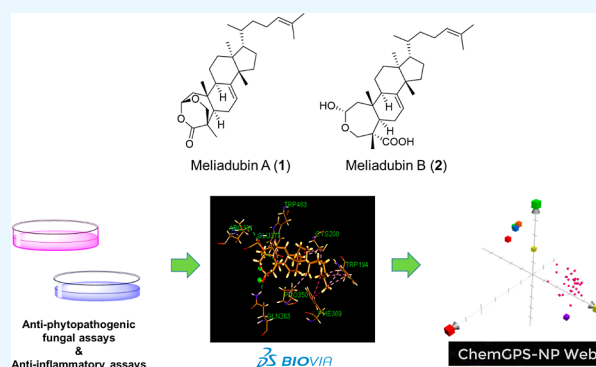
1. INTRODUCTION

Melia dubia Cav. (Meliaceae) is an indigenous and densely foliaceus tree distributed in Australia, South Asia, and Southeast Asia.[1] *M. dubia* is usually found at an altitude of 600−1800 m, on locations with heavy rainfall and high humidity, where it may reach a height of 25 m. It is considered as a valuable commodity due to its industrial suitability for timber, plywood, pulpwood, and fuel wood.[2] Moreover, the medicinal properties of *M. dubia* have been utilized as folk medicine. Leaves and fruits have been commonly used for alleviating skin infection. Furthermore, it has been deployed for illnesses related to the gastrointestinal tract, due to its anthelmintic, astringent, and colic properties.[3,4] A paste made from the raw fruits is used topically to treat scabies and maggot-infested sores, while a mixture of stem bark extract with opium has shown to reduce rheumatic pains.[2]

Several parts of *M. dubia* have been studied for their medicinal properties as they contain triterpenoids, alkaloids, flavonoids, anthraquinones, glycosides, tannins, and various essential oils.[2,5,6] Limonoids-rich ethanolic extract of *M. dubia* fruits was found to be an effective hypoglycemic agent with the

effect of reducing blood glucose level in vivo.[4] Meliastatins, a group of euphane-type limonoids, isolated from the bark showed antineoplastic activity by strongly inhibiting the growth of P388 lymphocytic leukemia cell line with ED_{50} $1.7−5.6\ \mu M$.[1] Another limonoid, (3α,8R,9S,20R,24S)-20,24-epoxytirucalla-3,25-diol, identified from the dried fruit displayed excellent antiphytopathogenic activity against the fungi *Magnaporthe oryzae* and *Sclerotium rolfsii*.[7] An ethanolic extract of its seeds was suggested to attenuate quorum sensing of uropathogenic *Escherichia coli* based on studies in vitro and in silico.[8] A high flavonoid content of an ethanolic extract from the leaves have been demonstrated to contribute to antioxidant and cutaneous wound healing activities by lowering nitric oxide radical scavenging and accelerating wound epithelialization,
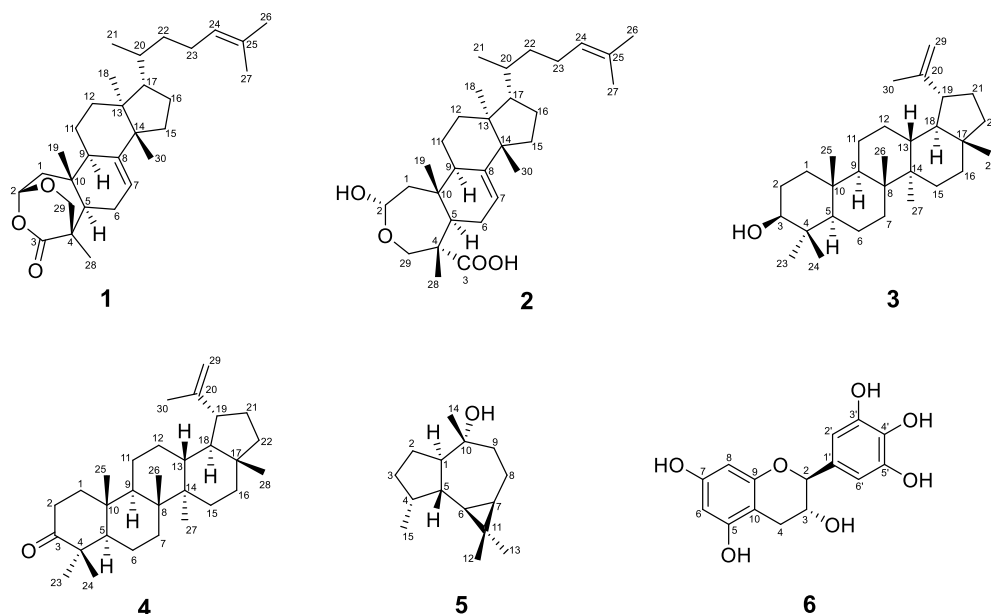
Figure 1. Structures of isolates 1−6.

respectively.[9] An ethyl acetate extract of *M. dubia* leaves showed a significant antimicrobial activity against both human and plant pathogenic microbes, such as *Bacillus cereus*, *E. coli*, *Fusarium oxysporum*, *Klebsiella* sp., *Macrophomina phaseolina*, *Rhizoctonia solani*, *Salmonella typhi*, *S. rolfsii*, and *Staphylococcus epidermidis*.[10]

In this study, a phytochemical investigation on the methanolic extract of dried bark of *M. dubia* led to the isolation of six secondary metabolites. Two new compounds, meliadubins A and B (1 and 2), present a rearranged 2,3-*seco*-tirucallane triterpenoid skeleton. Additionally, two pentacyclic triterpenoids lupeol (3)[11] and lupenone (4),[12] a sesquiterpenoid (−)-globulol (5),[13] and a flavanol (−)-gallocatechin (6)[14] were isolated and identified (Figure 1). A plausible biosynthetic pathway of 1 and 2 through a Baeyer−Villiger oxidation mechanism was proposed. Isolates were subjected to antineutrophilic inflammatory and antiphytopathogenic fungal assays individually using in vitro models.

Furthermore, isolates were analyzed alongside a selected set of clinically used and approved anti-inflammatory drugs and fungicide agents using chemical global positioning system for natural products (ChemGPS-NP), a global model of physical-chemical property space, as implemented in ChemGPS-NP$_{web}$ (https://chemgps.bmc.uu.se).[15,16] Additionally, molecular docking experiments were conducted based on the "key in a lock" concept with an idea of the specificity of an enzyme for its substrates with complementary geometries in structure-based drug discovery.[17,18]

2. RESULTS AND DISCUSSION

2.1. Purification and Structural Elucidation of Bioactive Components.
The methanolic extract of *M. dubia* was partitioned for chemical separation based on their polarities. Meliadubin A (1) and compounds 3−5 were isolated from the *n*-hexane partitioned layer, while meliadubin B (2) and compound 6 were obtained from the ethyl acetate partitioned layer.

Compound 1 was obtained as a white powder. Its molecular formula was confirmed as $C_{30}H_{46}O_3$ using HRESIMS data (*m/*

z 477.33405 [M + Na]$^+$, calcd 477.33392), which required eight degrees of unsaturation. Its IR spectrum exhibited strong absorption at 1753 cm^{-1} for ester moiety, an ether absorption at 1215 cm^{-1}, and strong absorptions at 986 and 736 cm^{-1} indicating the availability of disubstituted alkenes. The UV spectrum displayed an λ_{max} value at 217 nm. The ^{1}H NMR spectrum showed six tertiary methyl groups, one secondary methyl group, 16 methylene protons, two oxymethylene protons, an oxymethine proton, two olefinic methine protons, and four methine protons. The ^{13}C NMR and DEPT analysis revealed seven methyls (δ_C 27.4, C-30; δ_C 25.7, C-27; δ_C 22.0, C-18; δ_C 18.4, C-28; δ_C 18.3, C-21; δ_C 17.6, C-26; δ_C 15.3, C-19), eight methylenes (δ_C 45.6, C-1; δ_C 36.1, C-22; δ_C 34.0, C-15; δ_C 33.5, C-12; δ_C 28.1, C-16; δ_C 25.5, C-6; δ_C 25.0, C-23; δ_C 18.4, C-11), an oxymethylene (δ_C 66.5, C-29), four methines (δ_C 52.9, C-17; δ_C 50.0, C-9; δ_C 46.4, C-5; δ_C 35.8, C-20), an oxymethine (δ_C 98.7, C-2), two olefinic methines (δ_C 125.1, C-24; δ_C 118.1, C-7), two olefinic carbons (δ_C 146.6, C-8; δ_C 131.0, C-25), four quaternary carbons (δ_C 51.1, C-14; δ_C 44.2, C-4; δ_C 43.3, C-13; δ_C 36.2, C-10), and a carboxylic group (δ_C 175.5, C-3) (Table 1).

The HMBC correlations from H-15, H-16 to C-14; from H-17 to C-12; from H$_3$-18 to C-12, C-13, C-14; and from H$_3$-30 to C-13, C-14, C-15 along with COSY correlations on H-9/H-11/H-12 confirmed the formation of ring C and ring D with attached methyl group on each of C-13 and C-14. Ring B was formed by HMBC from H-5 to C-9, C-10, and COSY on H-5/H-6/H-7. Moreover, ring B was determined as a cyclohexene after placement of an olefinic carbon at C-8 following HMBC from H$_3$-30 to C-8 and no available COSY between H-7 and H-9. Moreover, a 2-methyl-2-heptene side chain was connected to ring D via C-17 and C-20 bonds after COSY between H-20/H-21 and H-15/H-16/H-17/H-20/H-22/H-23/H-24, together with HMBC from H-26, H-27 to C-24, C-25, and from H-27 to C-26 (Figure 2).

The COSY on H-1/H-2 as well as HMBC from H-2, H-5 to C-3; from H-1 to C-10; and from H-5 to C-4 confirmed the position of the ester moiety at C-3 in ring A between an oxymethine carbon (C-2) and a quaternary carbon (C-4).

Table 1. ^{1}H and ^{13}C NMR Data of 1–2 (δ in ppm, J in Hz)^a

position		1		2	
		δ_H, mult. (J)	δ_C, mult	δ_H, mult. (J)	δ_C, mult
1	α	2.23 dd (15.0, 6.2)	45.6, CH$_2$	1.94 dd (12.6, 4.4)	42.9, CH$_2$
	β	1.80 d (15.0)		1.58 m	
2		5.75 d (6.2)	98.7, CH	4.95 dd (10.0, 4.4)	93.1, CH
3			175.5, C		177.1, C
4			44.2, C		51.4, C
5		2.07 br d (12.0)	46.4, CH	2.25 br d (13.6)	46.3, CH
6	α	2.15 m	25.5, CH$_2$	1.66 m	26.4, CH$_2$
	β	2.18 m		1.98 m	
7		5.27 t (2.2)	118.1, CH	5.22 t (2.2)	117.8, CH
8			146.6, C		144.7, C
9		2.40 m	50.0, CH	2.11 m	49.5, CH
10			36.2, C		37.6, C
11	α	1.52 m	18.4, CH$_2$	1.72 m	19.1, CH$_2$
	β	1.49 m		1.45 m	
12	α	1.76 m	33.5, CH$_2$	1.78 m	33.8, CH$_2$
	β	1.61 m		1.68 m	
13			43.3, C		42.9, C
14			51.1, C		51.4, C
15		1.45 m	34.0, CH$_2$	1.38 m	34.2, CH$_2$
16	α	1.25 m	28.1, CH$_2$	1.22 m	28.1, CH$_2$
	β	1.94 m		1.88 m	
17		1.42 m	52.9, CH	1.41 m	52.6, CH
18		0.77 s	22.0, CH$_3$	0.77 s	22.1, CH$_3$
19		1.11 s	15.3, CH$_3$	0.80 s	12.1, CH$_3$
20		1.39 m	35.8, CH	1.34 m	35.3, CH
21		0.85 d (6.3)	18.3, CH$_3$	0.85 d (6.2)	18.3, CH$_3$
22		1.01 m	36.1, CH$_2$	1.01 m	35.9, CH$_2$
23		1.87 m	25.0, CH$_2$	1.84 m	24.6, CH$_2$
		1.90 m		2.03 m	
24		5.07 t (7.1)	125.1, CH	5.06 t (7.2)	125.1, CH
25			131.0, C		130.5, C
26		1.58 s	17.6, CH$_3$	1.55 s	17.7, CH$_3$
27		1.66 s	25.7, CH$_3$	1.62 s	25.7, CH$_3$
28		1.06 s	18.4, CH$_3$	1.15 s	17.1, CH$_3$
29		4.30 d (10.7)	66.5, CH$_2$	4.19 d (12.5)	65.5, CH$_2$
		3.63 d (10.6)		3.10 d (12.5)	
30		0.97 s	27.4, CH$_3$	0.95 s	28.0, CH$_3$

^{a}Recorded in CDCl$_3$ (1) and DMSO-d_6 (2) at 400 MHz (^{1}H) and 100 MHz (^{13}C).

Thus, ring A was rearranged to be a 7-membered ring known as the 2,3-*seco*-tirucallane structure.[19] Moreover, the HMBC

from H-29 to C-2, C-3, and C-5 put an oxymethylene attached in between C-2 and C-4 to corroborate a bicyclo[3.1.1] structure in ring A. In addition, a methyl group was attached to each of C-4 and C-10 after HMBC found from H-28 to C-3, C-4; from H-5, H$_2$-29 to C-28; from H-19 to C-9, C-10; and from H-1, H-5 to C-19 (Figure 2). Thus, 2,3-*seco*-tirucallane bicyclo[3.1.1] structures were confirmed.

Based on the NOESY spectrum (Figure 3), the correlations between H-1β, H$_3$-19, and H-30 suggested that methyl groups at C-19 and C-30 were assigned in the β position, while the correlations between H-16β, H-17, and H$_3$-30 indicated that the 2-methyl-2-heptene side chain was confirmed as α-oriented. The NOESY correlations between H-1α, H-5, H-9, and H$_3$-18 confirmed methyl at C-18 and two protons in methines of C-5 and C-9 were set in the α position. An oxymethylene at C-29 was settled as β-oriented due to the NOESY correlation of H-1α with H-2. The obtained crystal of 1 confirmed its absolute stereochemistry through X-ray crystallography as 2*R*,4*S*,5*R*,9*R*,10*R*,13*S*,14*S*,17*S*,20*S* (Figure 4). Therefore, the structure of 1 was determined as 2,3-*seco*-tirucalla-2,3;2,29-diepoxy-7,24-diene-3-one, and it was named as meliadubin A.

Compound 2 was isolated as a colorless crystal with verified molecular formula as C$_{30}$H$_{48}$O$_4$ using HRESIMS data (*m/z* 495.34437 [M + Na]$^+$, calcd 495.34448), which required seven degrees of unsaturation. Its IR spectrum exhibited a broad absorption at 3397 cm^{-1} assigned as a carboxylic acid group and a secondary alcohol absorption at 1037 cm^{-1}. The NMR data of 2 were closely related to those of 1, except they were shifted on C-2 (δ_H 4.95 dd (10.0, 4.4), δ_C 93.1) to be a secondary hydroxyl moiety and C-4 (δ_C 51.2), which indicated that missing an oxymethylene bridge between C-2 and C-4 led to the breakage of bicyclo[3.1.1] structure and reduced one degree of unsaturation. The COSY correlations of 2 were similar to those of 1. The HMBC correlations from H$_3$-28 to C-3, C-4, and C-29 assigned the attachment of a methyl group at C-28 and a carboxyl group at C-3 to a quaternary carbon at C-4. While, the HMBC from H$_2$-29 to C-2 formed a hemiacetal moiety to corroborate 2,3-*seco*-tirucallane structure (Figure 2).

The NOESY correlations between H-1β, H-2, and H$_3$-28 confirmed the methyl group at C-28 as β-oriented, while a hydroxyl group at C-2 and a carboxyl group at C-3 were assigned as α-oriented (Figure 3). A crystal of 2 was obtained using a 1:1 methanol/acetone solution and was used to determine the absolute stereochemistry of 2 via X-ray crystallography as 2*S*,4*S*,5*R*,9*R*,10*R*,13*S*,14*S*,17*S*,20*S* (Figure
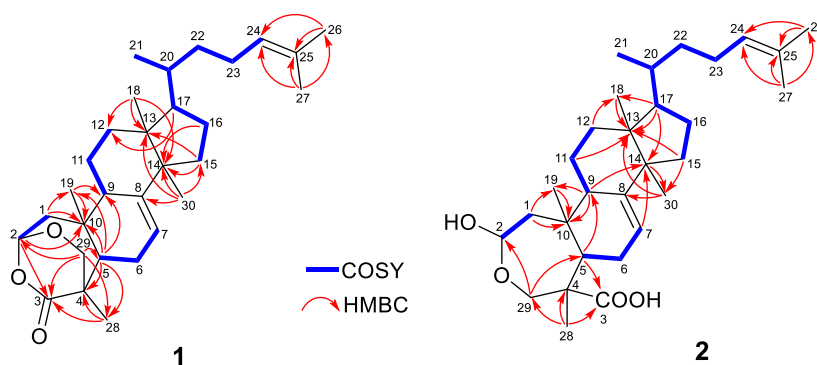
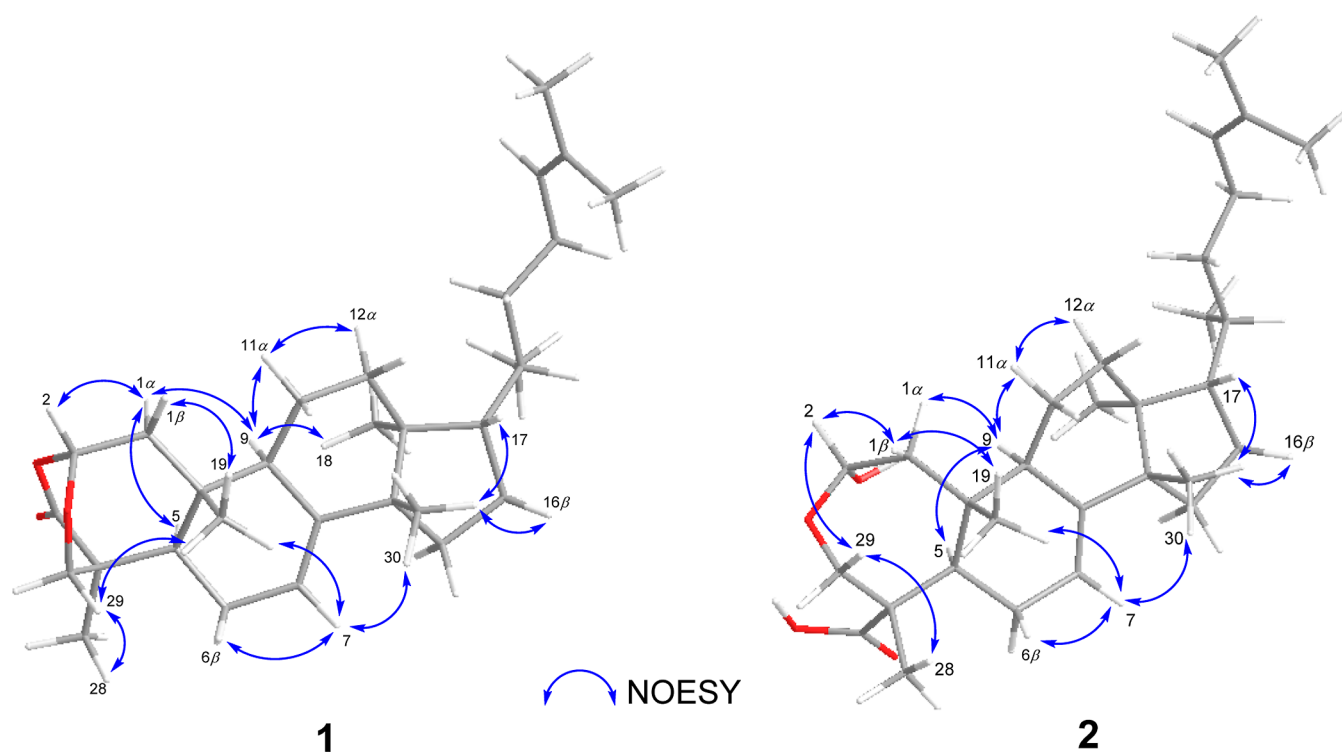**Figure 2.** Key COSY and HMBC correlations of 1 and 2.

Figure 3. Key NOESY correlations of **1** and **2**.

4). Hence, compound **2** was established as 2β-hydroxy-2,3-seco-tirucalla-2,29-epoxy-7,23-diene-3-oic acid and was named as meliadubin B.

Compounds **1** and **2** were regarded as natural products because the interchanges of lactonization reaction to form the special bicyclo ring do not easily happen in ordinary conditions. In general, it will react under higher temperature, catalysts, anhydride, and/or availability of better halogenic leaving group. Compounds **1** and **2** feature a 2,3-seco-tirucallane triterpenoid skeleton along with a 2-methyl-2-heptene side chain. The skeleton originates from tirucalla-7,24-dien-3β-ol based on the similarity of their relative configuration on methyl groups and side chain formation. Tirucalla-7,24-dien-3β-ol is formed through either mevalonate pathway or methylerythritol pathway, and commonly isolated from plants of the Meliaceae.[20] The biosynthetic pathway of **1** and **2** was started with the initial oxidation on C-2 and C-3 to create a tirucallane-type intermediate named tirucalla-7,24-dien-3-one with 1,2-diketone formation. Further oxidation at C-29 formed a primary alcohol. The Baeyer–Villiger oxidation transformed a ketone at C-2 into an ester, followed by a cleavage at ring A after hydration between C-2 and C-3 to create a 2,3-seco-tirucallane configuration.[19] Reduction of C-2 and C-3 turned both carboxyls into aldehydes. Compound **2** was formed through rearrangement of ring A after a hemiacetal reaction between methylene hydroxyl (C-29) and an aldehyde (C-2), then continued with oxidation on aldehyde at C-3. Esterification between α-hydroxyl (C-2) and α-carboxyl (C-3) corroborated a bicyclo[3.1.1] structure with an β-oriented oxymethylene (C-29) to complete the formation of **1** (Figure 5).

2.2. Antineutrophilic Inflammatory Activity. Neutrophils play an important role in the human immune system as a first line defense against bacterial infection. However, over-activation of neutrophils increases superoxide anion generation

and elastase release, which induce cytokine expression to secretes pro-inflammatory mediator.[21] Large numbers of activated neutrophil accumulation elicit tissue damage due to an excessive response to the inflammatory mediator. This circumstance may lead to organ impairment, especially during systemic inflammation.[22]

The anti-inflammatory evaluation was conducted using both superoxide anion generation and elastase release in fMLF/CB-induced human neutrophil assays on all isolates. Compound **2** exhibited the strongest anti-inflammatory effect among all isolates by inhibiting superoxide anion generation on neutrophils with EC_{50} 5.54 ± 0.36 μM. Moreover, compound **2** also showed 39.38 ± 8.69% inhibition toward elastase release at 10 μM. The other compounds displayed insignificant inhibition on both assays (Table 2). LY294002 (10 μM) was used as a positive control for these assays.[23]

Neutrophilic inflammation occurred after nitric oxide stimulation was produced by constitutive nitric oxide synthases (NOS) known as inducible NOS (iNOS). The inhibitory effect on iNOS gene expression in RAW 264.7 cells by a triterpenoid derivative has been reported previously.[24] Computational molecular docking simulations were performed to study involvement of iNOS by predicting the binding mode of **2** with 3E7G, a human inducible nitric oxide synthase (INOSOX).[25,26] The -CDOCKER energy and -CDOCKER interaction energy displayed suitable binding conformer with the values of −85.0283 and 47.1881 kcal mol^{-1}, respectively (Table 3).[27] The calculation results predicted **2** to bind into the active sites of human INOSOX 3E7G with a binding energy of −89.6757 kcal mol^{-1} through the formation of a hydrogen bond with the residue of GLU377 combined with a hydrophobic interaction with the residue of PRO350 (Figure 6 and Table 3). Both GLU377 and PRO350 have been suggested as essential active site residues of 3E7G in previous study of iNOS molecular docking.[26,28] In addition, an iNOS
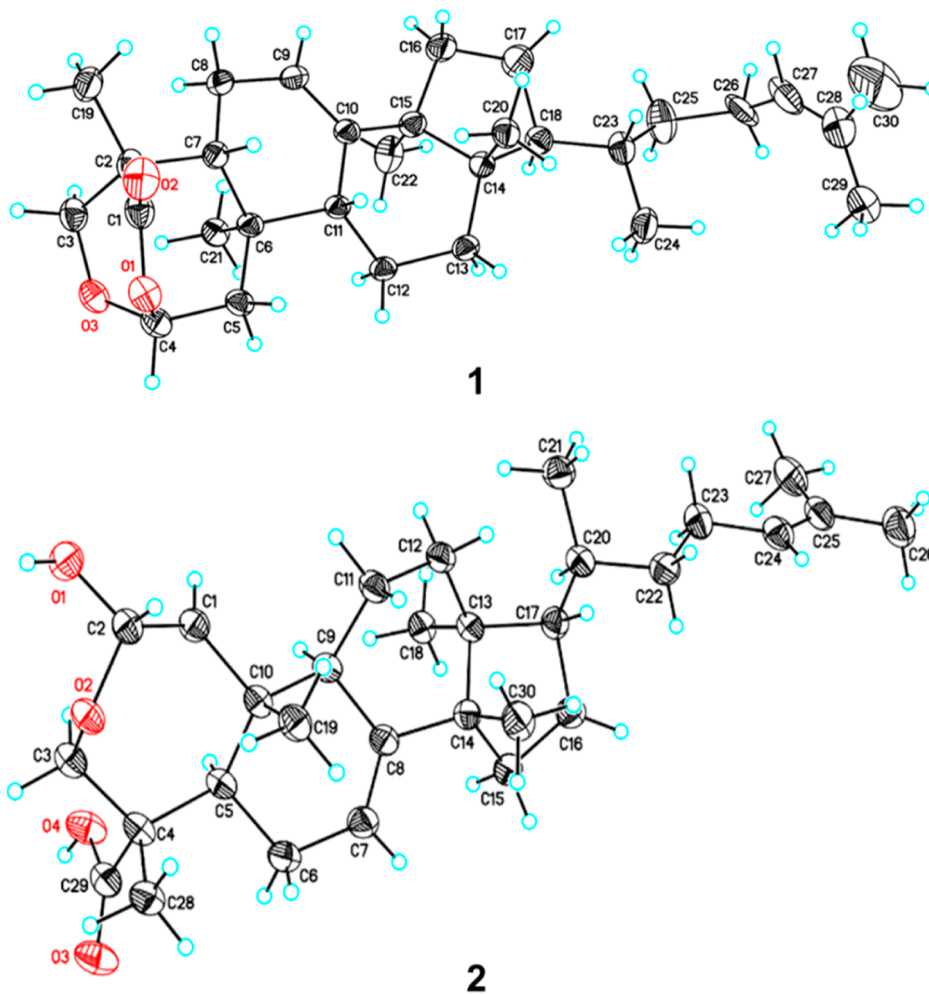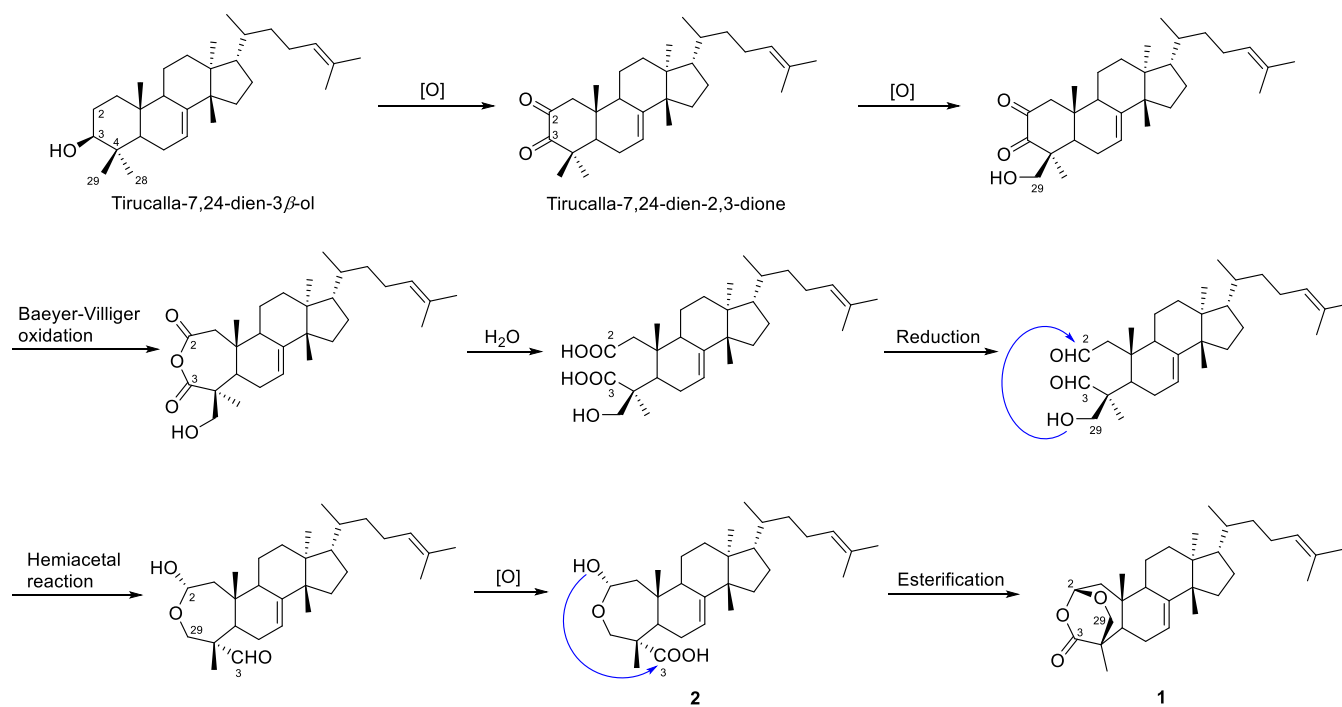
Figure 4. X-ray crystal diffraction structures of **1** and **2**.

Figure 5. Plausible biosynthetic pathways of **1** and **2**.

Table 2. Effects of Isolates on Superoxide Anion Generation and Elastase Release in fMLF/CB-Induced Human Neutrophils[a]

compounds	superoxide anion generation		elastase release
	inhibition (%)[b]	EC$_{50}$ (μM)[c]	inhibition (%)[b]
1	14.94 ± 4.41*		−38.52 ± 2.53***[d]
2	92.26 ± 4.76***	5.54 ± 0.36	39.38 ± 8.69*
3	25.85 ± 7.49*		6.75 ± 3.64
4*	21.89 ± 5.91		2.78 ± 1.37
5	32.15 ± 3.55***		18.17 ± 7.21
6	19.21 ± 4.31*		4.35 ± 7.09

[a]LY294002 (10 μM; $n = 4$) was used as positive control. It showed concentration necessary for 50% of inhibition (IC$_{50}$) of 1.54 ± 0.40 μM on superoxide anion generation and 3.27 ± 0.70 μM on elastase release. [b]Results are presented as mean ± SEM (n = 3 or 4) at 10 μM. The fMLF/CB induced cell responses are expressed as 100%. *$p < 0.05$, ***$p < 0.001$ compared with the basal (solvent only). [c]Concentration for 50% of maximal effective concentration (EC$_{50}$). [d]The minus sign (−) means the promoting effect of elastase release.

inhibitor (E)-2-cyano-N,3-diphenylacrylamide was used for positive controls in the initial molecular docking simulation against 3E7G.[28] It also bound to 3E7G through interaction with GLU377 and PRO350 residues (Figure S31 and Table S12, Supporting Information). Hence, the obtained results

suggested that **2** could be a promising compound, given the good docking results predicted for iNOS.

A ChemGPS-NP analysis was conducted to compare physical-chemical properties of isolates to those of approved anti-inflammatory drugs. The eight dimensional (8D) positions in chemical property space were calculated for **1−6** as well as a reference set of 34 selected active compounds from approved anti-inflammatory drugs. Due to dimensional constraints, only 3D plots can be conceived in our context, but 77% of the information is retained in the first three dimensions, PC1− PC3. PC1 (red axis) primarily contains size and volume parameters, PC2 (yellow axis) various aspects of aromaticity and conjugation-related parameters, and PC3 (green axis) solubility, lipophilicity and hydrogen-bond related parameters.[29] From the plot of PC1−PC3 of **1−6** and anti-inflammatory reference compounds (Figure 7), it can be concluded that all isolates, in particular, **1−4**, are fundamentally different from the selected reference set of anti-inflammatory drugs. Hence, there is a significant possibility that any exhibited anti-inflammatory activity is mediated by a novel binding mode. Thus, exploring possible anti-inflammatory mechanisms of actions of **2** may help in developing more active triterpenoids, which also exploit different mechanisms as compared to current approved drugs. Combining the results from the bioactivity assay, molecular docking, and ChemGPS-NP, compound **2** is suggested to be an agent for targeting

Table 3. Summary of Molecular Docking 2 Against Human INOSOX 3E7G (A), and 1 and 2 in Complex of Trihydroxynaphthalene Reductase 1YBV (B) With Their Respective Binding Energy and Interacting Amino Acid Residues[a]

| compounds	-CDOCKER energy (kcal mol^{-1})	-CDOCKER interaction energy (kcal mol^{-1})	binding energy (kcal mol^{-1})	residues involved in hydrogen bond interaction (bond distance, Å)	residues involved in hydrophobic interaction (bond distance, Å)
A. 3E7G					
2	−85.028	47.1881	−89.676	ARG381 (2.79924) GLN263(2.07985) **GLU**377 (2.22915)	CYS200 (4.08355, 4.00815, 4.13450) PHE369 (5.11756, 4.91489) **PRO**350 (5.0065) TRP194 (4.45417, 3.92766, 4.22684, 4.84535) TRP463 (5.17759, 4.61087)
B. 1YBV					
1	−98.537	48.5794	−109.15	ASN114 (2.71559) GLY116 (2.90214)	CYS220 (4.75093) ILE41 (3.96895) ILE41 (4.28084) ILE41 (4.56010) ILE211 (4.87514) MET162 (4.69910) MET215 (4.21317, 4.45760, 4.34386, 3.50092, 5.04226) PRO208 (3.82664) PRO208 (4.77133) TRP243 (4.02177) TYR178 (4.48733) **TYR223** (**4.67390, 3.78947**)
2	−104.6	51.8032	−105.15	ILE211 (2.27122) THR213 (3.00157) **TYR**223 (2.00893)	ALA61 (3.64718) ARG39 (4.31627) ILE41 (4.36538, 4.38261, 4.63565) MET162 (4.21135) MET215 (3.77924, 4.63520, 4.62467, 3.68477) PRO208 (4.26896) PRO208 (4.91950)

[a]Active sites of amino acids are bolded.
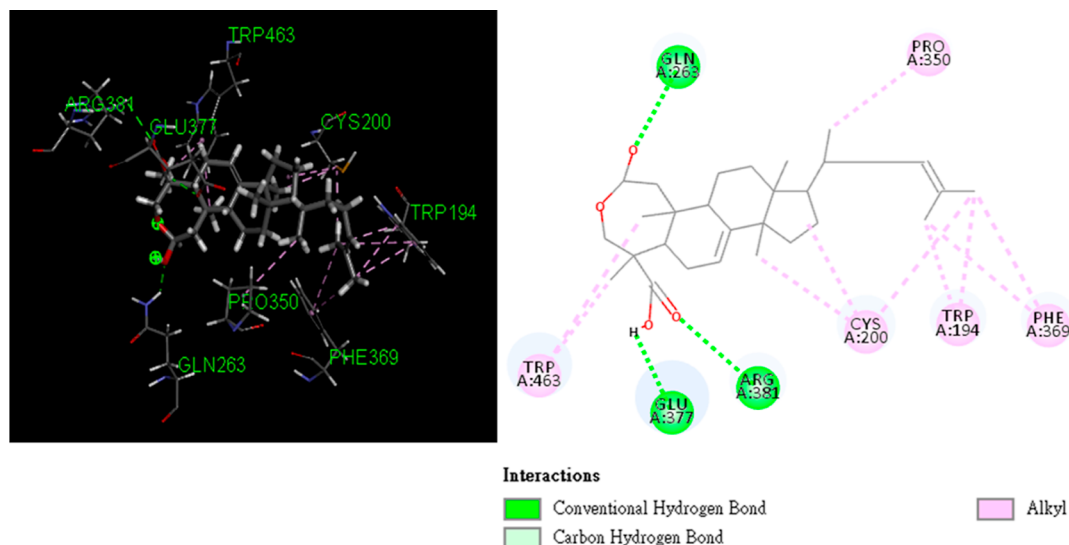
Figure 6. Molecular docking of **2** in complex with human INOSOX (3E7G).
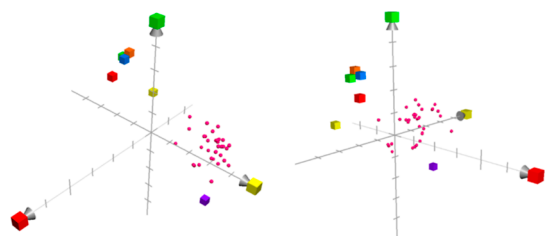

Figure 7. ChemGPS-NP analysis of **1−6** (colored cubes) and clinically approved anti-inflammatory drugs (magenta dots). The three-dimensional axes represent principal component properties, consisting of PC1 (red axis), PC2 (yellow axis), and PC3 (green axis).

iNOS and a lead candidate for further development as an anti-inflammatory drug.

2.3. Activity Against Phytopathogenic Fungi. The six isolates **1−6** were subjected to an in vitro evaluation of activity against six phytopathogenic fungi, namely, *Colletotrichum acutatum*, *Colletotrichum gloeosporioides*, *F. oxysporum*, *M. oryzae*, *Phytophthora capsici*, and *Phytophthora* sp. *M. oryzae*, a filamentous Ascomycete fungus, has been known for causing rice blast disease that affects global rice production by

destroying million hectares of rice fields in Asia and United States annually.[30] Additionally, the Oomycete genus *Phytophthora* spp. include several well-known phytopathogenes, such as *Phytophthora infestans*, which caused the Irish potato famine in the 1840s, and *P. capsici*, the cause of rotting root and blighting fruit on chili pepper.[31] In this perspective, finding an agent that inhibits the growth of *M. oryzae* and species of *Phytophtora* may become pivotal to achieve a more sustainable food security. Both **1** and **2** showed an inhibition against *M. oryzae* in a dose-dependent manner with IC_{50} values of 137.20 ± 9.55 and 182.50 ± 18.27 μM, respectively (Figure 8 and Table S1, Supporting Information). Compound **2** also reduced the level of growth of *P. capsici* and *Phytophthora* spp. at 500 μg/mL by $39.20 \pm 10.98\%$ and $45.71 \pm 3.99\%$ inhibitions, respectively (Table S2, Supporting Information).

Molecular docking experiments were conducted on **1** and **2** to determine their binding modes and to predict their modes of action. Initially, both compounds were docked against four different target enzymes of scytalone dehydratase (1STD), trihydroxynaphthalene reductase (1YBV), trehalose-6-phosphate synthase 1 (6JBI), and isocitrate lyase enzyme (5E9G) that are responsible for the cellular process or pathogenicity of fungi.[32] The results showed both compounds only have
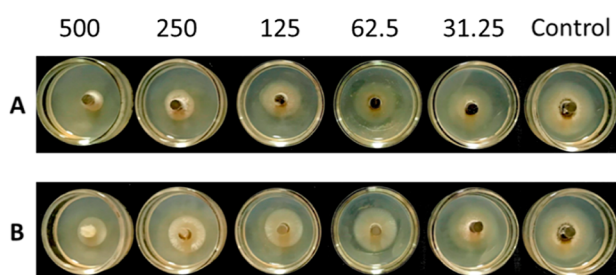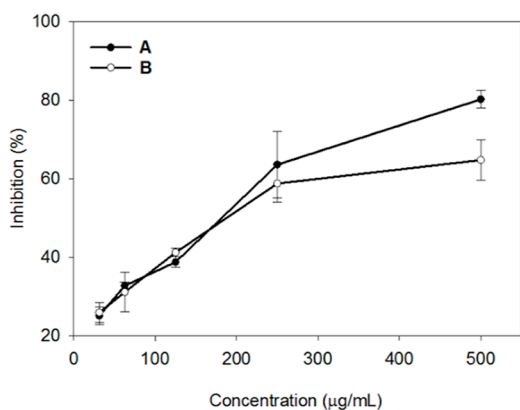

Figure 8. In vitro antiphytopathogenic fungal activity of **1** (**A**) and **2** (**B**) against *Magnaporthe oryzae* at a concentration range of 31.25−500 μg/mL, $p < 0.05$. Inhibition (%) was compared with PDA alone. Difenoconazole (250 μg/mL) served as a positive control and completely inhibited mycelial growth of *M. oryzae*.
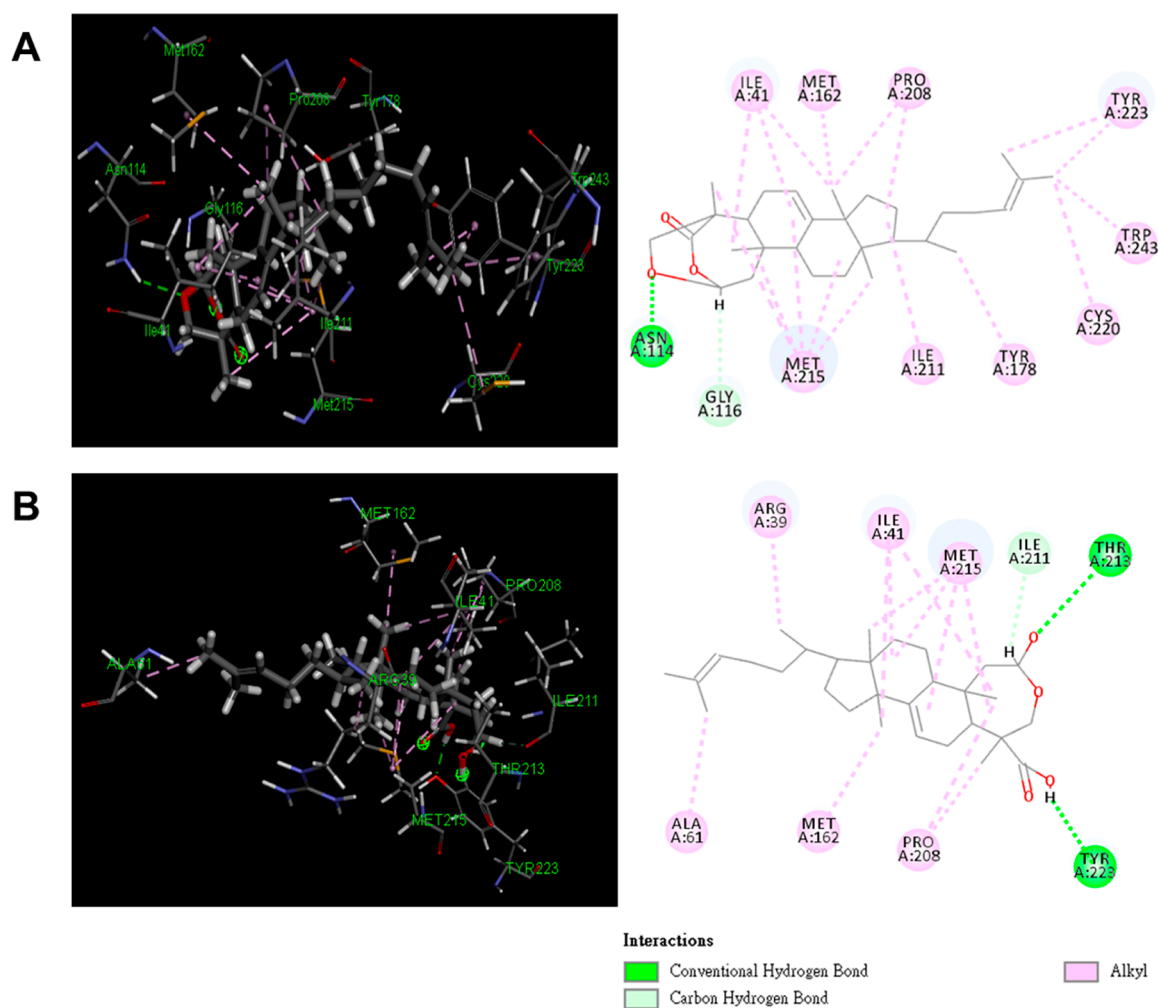
Figure 9. Molecular docking of **1** (**A**) and **2** (**B**) in complex with trihydroxynaphthalene reductase (1YBV).

interaction with 1YBV and did not show available interaction pose with each of 1STD, 6JBI, and 5E9G (Figure S33, Supporting Information). Trihydroxynaphthalene reductase (1YBV) is an essential enzyme catalyzing the conversion of trihydroxynaphthalene to vermelone during melanin biosynthesis.[32] Melanin is a polymer-type structure composed by series of aromatic rings that is deposited in fungi cell wall providing defense against environmental stress to enhance fungi survival ability and growth in the environment.[33] It can absorb ultraviolet radiation to allow fungi to survive in extreme temperature and make the cell wall structure stronger to be more resistant from enzymatic degradation.[34] Moreover, melanin reduces the antifungal activities of several fungicides on fungi by decreasing cell wall permeability.[35,36] Therefore, the molecular docking on 1YBV, an essential enzyme on the melanin biosynthetic pathway, represents one of the targets for development of fungicides.

Further molecular docking experiments on **1** and **2** against 1YBV were conducted to predict their antifungal potential as melanin biosynthesis inhibitors. The -CDOCKER energy and -CDOCKER interaction energy showed suitable binding conformers for both **1** and **2** (Table 3).[27] Compound **1** bound to the active site of 1YBV with a binding energy value of -109.1515 kcal mol^{-1} through a hydrophobic interaction with the residue of TYR223, while **2** had a binding energy value of -105.1527 kcal mol^{-1} through a hydrogen bond with the

residue of TYR223 (Figure 9 and Table 3). Additionally, the result was supported by the molecular docking of 1-(2-bromo-2-nitrovinyl)-4-ethylbenzene (positive control) toward 1YBV, which bound through interaction with the residue of TYR223 (Figure S34 and Table S13, Supporting Information).[37] The binding sites of **1** and **2** are correlated with those of the positive control. In previous study, TYR223 was regarded as a key active site of 1YBV for ligand−protein interaction in antifungal molecular docking. Compound possessed hydrophobic interaction with TYR223 and had lower binding energy and was favored to have higher binding affinity with 1YBV.[32,37] Thus, compound **1** can be inferred to have a better and more stable interaction with 1YBV than that of **2**.

Compounds **1** and **2** were also analyzed using ChemGPS-NP to predict their activities against phytopathogenic fungi as compared to a selected set of commercially available fungicide agents. Based on the ChemGPS-NP plotting, both **1** and **2** have fundamentally different physical-chemical properties compared to those of the reference set. Interestingly, we noted that most of the agents used against phytopathogenic fungi had negative PC1 values, indicating a comparably small molecular size and weight, and positive PC2 values relating to more aromatic related properties. These features are different from both **1** and **2**, results indicated that **1** and **2** might possess physical-chemical properties different from those of commercially used agents against phytopathogenic fungi (Figure 10).
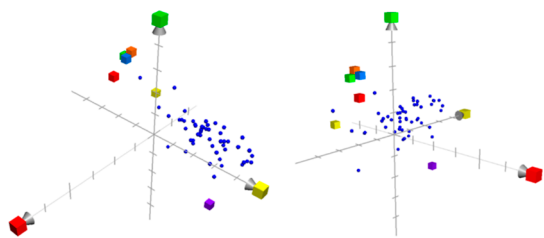
Figure 10. ChemGPS-NP analysis of **1**−**6** (colored cubes) and fungicide agents (blue dots). The three-dimensional axes represent principal component properties, consisting of PC1 (red axis), PC2 (yellow axis), and PC3 (green axis).

3. CONCLUSIONS

In conclusion, the phytochemical investigation on a methanolic extract of *M. dubia* barks leads to isolation of two new and active 2,3-*seco*-tirucallane triterpenoids, meliadubins A (**1**) and B (**2**). Compound **2** exhibited strong anti-inflammatory effect by inhibiting superoxide anion generation on neutrophils and indicated an interaction with the active sites of 3E7G from molecular docking. Moreover, both **1** and **2** showed strong inhibition against *M. oryzae* in a dose-dependent manner and showed interactions with the active site of 1YBV on molecular docking simulations. Bioactivity studies in combination with ChemGPS-NP and molecular docking in silico prediction experiments revealed that both **1** and **2** have the potency and properties to be developed as anti-inflammatory drugs or agents against phytopathogenic fungi exploiting novel modes of action.

4. METHODS

4.1. General Experimental Procedures. Silica gel (Silica gel 60, 0.040−0.200 nm; Merck KGaA, Darmstadt, Germany) and C_{18} silica gel (Merck KGaA, Darmstadt, Germany) were used for column chromatography. Silica gel-precoated TLC plates (Kieselgel 60 F254 and RP-18 F254, Merck KGaA, Darmstadt, Germany) were used. HPLC analyses were performed using a Shimadzu LC-20AT VP (Shimadzu Inc., Kyoto, Japan) pump interface equipped with a Shimadzu SPD-10VP UV−vis detector. Luna C_{18} preparative column (Phenomenex, 250 × 10.00 mm × 5 μm) was used. NMR spectra were obtained on a JEOL NM-ECS 400 NMR (JEOL Ltd., Tokyo, Japan). UV spectra were obtained on a JASCO V-530 ultraviolet spectrophotometer (JASCO Corp., Tokyo, Japan). IR spectra were obtained on an FT-IR-4100 JASCO spectrophotometer (JASCO Corp., Tokyo, Japan). Optical rotations were measured by using a JASCO P-2000 digital polarimeter (JASCO Corp., Tokyo, Japan). Melting points were measured using a Stuart SMP30 melting point (Cole-Palmer Ltd., Staffordshire, United Kingdom). Electrospray-ionization mass spectrometry (ESIMS) data were collected on a Waters micromass ZQ mass spectrometer (Waters Corp., Milford, MA, USA). High-resolution ESIMS (HR-ESIMS) data were acquired using a Bruker Daltonics APEX II mass spectrometer FT-ICR/MS instrument (Bruker Daltonics, Billerica, MA, USA). X-ray crystallographic analyses were carried out using Bruker AXS D8 Venture Photon III_C28 single-crystal XRD equipped with an Oxford cryostream 800+ (Bruker Corp., Billerica, MA, USA) and an Oxford Gemini dual system single-crystal XRD equipped with a cryojet (Oxford Instruments, Abingdon, United Kingdom).

4.2. Plant Material. The barks of *M. dubia* were collected in August 2018 from the Pu Huong Nature Reserve, Nghe An province, Vietnam, and identified by Nguyen Quoc Binh from the Institute of Ecology and Biological Resources, Vietnam Academy of Science and Technology. A voucher specimen (TDT-20180818) was deposited at the herbarium of the School of Chemistry, Biology and Environment, Vinh University, Vietnam.

4.3. Extraction and Isolation. The dried bark of *M. dubia* (12.5 kg) was extracted with methanol (20.0 L × 3) at 45 °C. Then, it was concentrated under vacuum to yield a crude extract (836.5 g). The crude extract was suspended in water (10.0 L) and subsequently partitioned successively by *n*-hexane (5.0 L × 3), ethyl acetate (5.0 L × 3), and *n*-butanol (5.0 L × 3) to yield the *n*-hexane partitioned layer (192.5 g), ethyl acetate partitioned layer (258.0 g), and *n*-butanol partitioned layer (96.8 g), respectively. The *n*-hexane layer was separated using silica column chromatography eluted with a stepwise gradient of *n*-hexane/ethyl acetate (50:1−1:1 v/v) to afford 8 main fractions (H.1 to H.8). Fraction H.3 (42.8 g) was subjected to a silica gel column with a dichloromethane/methanol (40:1−5:1 v/v stepwise) to obtain 9 subfractions (H.3.1 to H.3.9). Compounds **4** (151.2 mg) and **5** (307.7 mg) were obtained from subfraction H.3.3 (7.5 g) after being purified using silica column chromatography eluted with *n*-hexane/acetone (20:1−3:1 v/v stepwise). Compound **3** (74.2 mg) was isolated from subfraction H.3.5 (4.7 g) by silica column chromatography eluted with *n*-hexane/ethyl acetate (15:1−2:1 v/v stepwise). Fraction H.4 (27.6 g) was subjected to silica column chromatography eluted with *n*-hexane/acetone (20:1−1:1 v/v stepwise) to provide 10 subfractions (H.4.1−H.4.10). Subfraction H.4.5 (1.1 g) was separated by HPLC with a Luna C_{18} preparative column (methanol/water 1:4; 2.0 mL/min) to give **2** (291.9 mg). The ethyl acetate partitioned layer was eluted with a stepwise gradient of chloroform/methanol (100:0−0:100 v/v) to afford 9 main fractions (E.1−E.9). Fraction E.2 (27.1 g) was further separated using silica column chromatography eluted with *n*-hexane/ethyl acetate (25:1−1:1 v/v stepwise) to afford 8 subfractions (E.2.1−E.2.8). Compound **1** (75.7 mg) was isolated from subfraction E.2.7 (94.8 mg) by using HPLC with a Luna C_{18} preparative column (acetonitrile/water 7:3; 2.0 mL/min). Fraction E.5 (26.4 g) was subjected to silica column chromatography eluted with chloroform/methanol (20:1−3:1 v/v stepwise) to give 5 subfractions (E.5.1−E.5.5). Compound **6** (425.3 mg) was yielded from subfraction E.5.4 (2.1 g) by silica column chromatography eluted with chloroform/methanol (7:1, 4:1, 1:1 v/v stepwise).

4.3.1. Meliadubin A (1). Colorless crystal; mp 142−148 °C; $[\alpha]_D^{25}$ − 89.4 (*c* 0.37, CH$_2$Cl$_2$); UV (CH$_2$Cl$_2$) λ_{max} (log ε) 217 (1.79) nm; IR ν_{max}: 2948, 2359, 1753, 1457, 1380, 1267, 1215, 1177, 1148, 1096, 986, 937, 736 cm^{-1}; NMR data (Table 1); HRESIMS *m/z*: 477.33405 [M + Na]$^+$ calcd for C$_{30}$H$_{46}$NaO$_3$, 477.33392.

4.3.2. Meliadubin B (2). White powder; mp 194−202 °C; $[\alpha]_D^{25}$ + 25.5 (*c* 0.33, CH$_3$OH); UV (CH$_3$OH) λ_{max} (log ε) 217 (1.85) nm; IR ν_{max}: 3397, 2951, 1706, 1636, 1449, 1375, 1242, 1144, 1088, 1037, 1026, 970, 879, 777, 735 cm^{-1}; NMR data (Table 1); HRESIMS *m/z*: 495.34437 [M + Na]$^+$ calcd for C$_{30}$H$_{48}$NaO$_4$, 495.34448.

4.4. X-ray Crystallographic Analyses. Single crystal of **1** (C$_{30}$H$_{46}$O$_3$) was obtained in a solution of methanol/acetone/ethyl acetate 1:1:1 and analyzed on a Bruker AXS D8 Venture

Photon III_C28 single-crystal XRD instrument equipped with an Oxford cryostream 800+ with Cu Kα radiation (λ = 1.54178 Å). The crystal was kept at 100.00 K during data collection. Crystal data of **1**: orthorhombic, space group P_{2_1}(#4), a = 6.7509(3) Å, b = 12.0684(5) Å, c = 32.0888(13) Å, V = 2614.36(19) Å3, Z = 4, T = 100.00 K, μ(Cu Kα) = 0.557 mm^{-1}, D_{calc} = 1.155 Mg/m^3, 35,303 reflections measured (2.754° $\leq$ 2θ $\leq$ 79.058°), 5497 unique observation (R_{int} = 0.0703), which were used in all calculations. The final R_1 was 0.0732 ($I > 2\sigma(I)$), and wR_2 was 0.2021 (all data). Crystal size: 0.200 × 0.200 × 0.020 mm^3; Flack parameter = −0.16(14) (Table S6, Supporting Information).

Single crystals of **2** ($C_{30}H_{47}O_4$) were obtained in a solution of methanol/acetone 1:1 and analyzed on an Oxford Gemini dual system single-crystal XRD equipped with cryojet with Cu Kα radiation (λ = 1.54178 Å). The crystal was kept at 108.00 K during data collection. Crystal data of **2**: orthorhombic, space group P_{2_1}(#4), a = 6.7780(5) Å, b = 11.6549(6) Å, c = 34.199(2) Å, V = 2701.7(3) Å3, Z = 4, T = 108.00 K, μ(Ga Kα) = 0.584 mm^{-1}, D_{calc} = 1.160 Mg/m^3, 10,533 reflections measured (4.007°$\leq$ 2θ $\leq$ 67.997°), 4236 unique observation (R_{int} = 0.0440), which were used in all calculations. The final R_1 was 0.0560 ($I > 2\sigma(I)$), and wR_2 was 0.1567 (all data). Crystal size: 0.250 × 0.150 × 0.100 mm^3; flack parameter = 0.09(19) (Table S8, Supporting Information).

4.5. Isolation of Human neutrophils. This study was approved by Institutional Review Board of Chang Gung Memorial Hospital (IRB no. 201802192A3) and written informed consent was obtained from each healthy volunteer. The study was conducted according to the guidelines of the Declaration of Helsinki. According to the standard method of dextran sedimentation, the neutrophils were obtained from peripheral blood using an established protocol.[21]

4.6. Superoxide Anion Generation Assay and Elastase Release Inhibition Assays. The determination of the superoxide anion generation level by the neutrophil activation was based on the ferricytochrome *c* reduction as described previously.[38] Changes in absorbance with the reduction of ferricytochrome *c* at 550 nm were continuously monitored using a U-3010 spectrophotometer (Hitachi, Tokyo, Japan) with constant stirring. LY294002 (10 μM), a phosphoinositide 3-kinase inhibitor, was used as a positive control.

4.7. In Vitro Antiphytopathogenic Fungal Assay. The in vitro assay against phytopathogenic fungi was based on the evaluation of mycelial growth of the tested phytopathogenic fungi using poisoned-food technique.[39] Six species of phytopathogenic fungi, including *M. oryzae*, *C. acutatum*, *C. gloeosporioides*, *F. oxysporum*, *P. capsici*, and *Phytophthora* spp., were used in this assay. The tested compounds were dissolved in DMSO (0.25% Tween 20), then amended in the molten PDA in the 4.0 cm Petri dishes to yield the final concentrations of 250.0 and 500.0 μg/mL. After PDA was treated and became solid in the Petri dishes, an inoculum of test fungus (a 4.0 mm agar plug of 6−8 days old cultures of tested fungus) was inoculated at the center of each Petri dish. The Petri dishes containing PDA alone were used as negative controls. The inoculated Petri dishes were incubated at 25 °C for 4 days in an incubator. Each treatment was conducted three times, and the experiment was repeated at least twice. Difenoconazole (250 μg/mL) served as a positive control and completely inhibited the mycelial growth of *M. oryzae*. The inhibitory effectiveness was calculated according to the formula as follows:

$$\text{Inhibitory effectiveness (\%)} = \frac{D_{control} - D_t}{(D_{control} - 4)} \times 100\%$$

$D_{control}$: the diameter of mycelial growth in control plates (mm). D_t: the diameter of mycelial growth in the plate treated with test compound (mm). 4 (mm): the diameter of PDA agar plugs of fungal inoculum.

4.8. In Silico Prediction. Discovery Studio (Dassault Systemes, Velizy-Villacoublay, France) software was utilized for the molecular docking experiment. The 3E7G and 1YBV proteins data were downloaded from Protein Data Bank Web site (https://www.rcsb.org/) for molecular docking studies. The energy of the target proteins and ligand were minimized through the CHARMm-based smart minimizer method. The CHARMm-based DOCKER (CDOCKER) of BIOVIA Discovery Studio was used for the initial molecular docking experiment. The "Calculate Binding Energy" protocol of Discovery Studio was applied for calculating binding energies of ligand−receptor interactions after molecular docking completed. The -CDOCKER_ENERGY and -CDOCKER_-INTERACTION_ENERGY were used to find a docked pose, which gave the best binding affinity of the ligand to the receptor protein. The best binding affinity was interpreted as the best bonding stability between protein−ligand complexes.[26]

4.9. ChemGPS-NP Analysis. The ChemGPS-NP scores of isolated compounds and selected reference compounds were calculated from SMILES notations using the online tool ChemGPS-NP$_{Web}$ (http://chemgps.bmc.uu.se).[40] The SMILES notations for isolated compounds were derived using ChemBioDraw Professional version 17.0, while the reference sets for anti-inflammatory drugs and fungicide agents were acquired from the Drugbank database (https://go.drugbank.com/), and IUPAC Pesticides Properties database (https://sitem.herts.ac.uk/aeru/iupac/index.htm). The software Grapher 2.5 software was used for creating the 3D plots. The three ordinate axes represented size, shape, and polarizability (PC1, red axis); aromaticity and conjugation-related properties (PC2, yellow axis); and lipophilicity, polarity, and hydrogen bond capacity (PC3, green axis).[15] The six isolated compounds were marked as a blue cube (**1**), red cube (**2**), green cube (**3**), orange cube (**4**), yellow cube (**5**), and purple cube (**6**) (Table S3, Supporting Information). The 34 clinically approved drugs that were used as reference drugs for the physical-chemical analysis of anti-inflammatory properties were plotted using small magenta dots (Table S4, Supporting Information).[41−43] While, the 50 fungicides were used as reference and plotted using small blue dots (Table S5, Supporting Information).[44,45]

■ ASSOCIATED CONTENT

ⓢ Supporting Information

The Supporting Information is available free of charge at https://pubs.acs.org/doi/10.1021/acsomega.3c04657.

> Structural elucidation of **3−6**; antiphytopathogenic fungal assay data; ChemGPS-NP calculation data and plotting; and NMR, HRESIMS, ESIMS, IR, and UV spectra of **1−6**; X-ray crystallography data of **1** and **2**; Molecular docking data of positive and negative controls (PDF)

X-ray crystallographic information file for **1** (CIF)

X-ray crystallographic information file for **2** (CIF)

■ AUTHOR INFORMATION

Corresponding Authors

Tran Dinh Thang − *Institute of Biotechnology and Food Technology, Industrial University of Ho Chi Minh City, Ho Chi Minh City 727000, Viet Nam*; Phone: +84-913049689; Email: thangtd@iuh.edu.vn

Fang-Rong Chang − *Graduate Institute of Natural Products, College of Pharmacy, Kaohsiung Medical University, Kaohsiung 807378, Taiwan; Drug Development and Value Creation Research Center and Department of Medical Research, Kaohsiung Medical University Hospital, Kaohsiung Medical University, Kaohsiung 807378, Taiwan;* ⬤ orcid.org/0000-0003-2549-4193; Phone: +886-7-3121101 # 2162; Email: aaronfrc@kmu.edu.tw; Fax: +886-7-3114773

Authors

Hieu Tran Trung − *Department of Chemistry, Vinh University, Vinh City 462030, Viet Nam*; ⬤ orcid.org/0000-0002-0639-4261

Kartiko Arif Purnomo − *Graduate Institute of Natural Products, College of Pharmacy, Kaohsiung Medical University, Kaohsiung 807378, Taiwan;* ⬤ orcid.org/0000-0003-0858-5368

Szu-Yin Yu − *Graduate Institute of Natural Products, College of Pharmacy, Kaohsiung Medical University, Kaohsiung 807378, Taiwan; Institute of Pharmacognosy, University of Szeged, Szeged 6720, Hungary*

Zih-Jie Yang − *Graduate Institute of Natural Products, College of Pharmacy, Kaohsiung Medical University, Kaohsiung 807378, Taiwan*

Hao-Chun Hu − *Graduate Institute of Natural Products, School of Traditional Medicine, College of Medicine, Chang Gung University, Taoyuan 333323, Taiwan; Graduate Institute of Natural Products, College of Pharmacy, Kaohsiung Medical University, Kaohsiung 807378, Taiwan; Institute of Pharmaceutical Chemistry, University of Szeged, Szeged 6720, Hungary*

Tsong-Long Hwang − *Graduate Institute of Natural Products, School of Traditional Medicine, College of Medicine, Chang Gung University, Taoyuan 333323, Taiwan; Research Center for Chinese Herbal Medicine, Research Center for Food and Cosmetic Safety, and Graduate Institute of Health Industry Technology, College of Human Ecology, Chang Gung University of Science and Technology, Taoyuan 333324, Taiwan; Department of Anesthesiology, Chang Gung Memorial Hospital, Taoyuan 333423, Taiwan;* ⬤ orcid.org/0000-0002-5780-3977

Nguyen Ngoc Tuan − *Institute of Biotechnology and Food Technology, Industrial University of Ho Chi Minh City, Ho Chi Minh City 727000, Viet Nam*

Le Ngoc Tu − *Faculty of Chemistry, Ho Chi Minh City University of Education, Ho Chi Minh City 749000, Viet Nam*

Dau Xuan Duc − *Department of Chemistry, Vinh University, Vinh City 462030, Viet Nam*

Le Dang Quang − *Institute for Tropical Technology, Vietnam Academy of Science and Technology (VAST), Hanoi 122000, Viet Nam*

Anders Backlund − *Research Group Pharmacognosy, Department of Pharmaceutical Biosciences, Uppsala University, Uppsala S-75124, Sweden;* ⬤ orcid.org/0000-0003-2043-4183

Complete contact information is available at: https://pubs.acs.org/10.1021/acsomega.3c04657

Author Contributions

∥H.T.T. and K.A.P. contributed equally to the work.

Notes

The authors declare no competing financial interest.

■ ACKNOWLEDGMENTS

■ REFERENCES

(1) Pettit, G. R.; Numata, A.; Iwamoto, C.; Morito, H.; Yamada, T.; Goswami, A.; Clewlow, P. J.; Cragg, G. M.; Schmidt, J. M. Antineoplastic agents. 489. Isolation and structures of meliastatins 1−5 and related euphane triterpenes from the tree *Melia dubia*. *J. Nat. Prod.* **2002**, *65* (12), 1886−1891.

(2) Nagalakshmi, M. A. H.; Thangadurai, D.; Anuradha, T.; Pullaiah, T. Essential oil constituents of *Melia dubia*, a wild relative of *Azadirachta indica* growing in the Eastern Ghats of Peninsular India. *Flavour Fragrance J.* **2001**, *16* (4), 241−244.

(3) Kathiravan, V.; Ravi, S.; Ashokkumar, S. Synthesis of silver nanoparticles from *Melia dubia* leaf extract and their in vitro anticancer activity. *Spectrochim. Acta A Mol. Biomol. Spectrosc.* **2014**, *130*, 116−121.

(4) Susheela, T.; Balaravi, P.; Theophilus, J.; Reddy, T. N.; Reddy, P. U. M. Evaluation of hypoglycaemic and antidiabetic effect of *Melia dubia* Cav. fruits in mice. *Curr. Sci.* **2008**, *94* (9), 1191−1195.

(5) Zhao, L.; Huo, C. H.; Shen, L. R.; Yang, Y.; Zhang, Q.; Shi, Q. W. Chemical constituents of plants from the genus *Melia. Chem. Biodivers.* **2010**, *7* (4), 839−859.

(6) Fan, W.; Fan, L.; Wang, Z.; Yang, L. Limonoids from the genus *Melia* (Meliaceae): phytochemistry, synthesis, bioactivities, pharmacokinetics, and toxicology. *Front. Pharmacol* **2022**, *12*, 795565.

(7) Tan, T. N.; Trung, H. T.; Dang, Q. L.; Thi, H. V.; Vu, H. D.; Ngoc, T. N.; Do, H. T. T.; Nguyen, T. H.; Quang, D. N.; Dinh, T. T. Characterization and antifungal activity of limonoid constituents isolated from Meliaceae plants *Melia dubia, Aphanamixis polystachya*, and *Swietenia macrophylla* against plant pathogenic fungi in vitro. *J. Chem.* **2021**, *2021*, 4153790.

(8) Ravichandiran, V.; Shanmugam, K.; Solomon, A. P. Screening of SdiA inhibitors from *Melia dubia* seeds extracts towards the hold back of uropathogenic *E. coli* quorum sensing-regulated factors. *Med. Chem.* **2013**, *9* (6), 819−827.

(9) Thangavel, P.; Pathak, P.; Kuttalam, I.; Lonchin, S. Effect of ethanolic extract of *Melia dubia* leaves on full-thickness cutaneous wounds in Wistar rats. *Dermatol. Ther.* **2019**, *32* (6), No. e13077.

(10) Nikkitha, J. P.; Suresh, P.; Kameshwaran, S.; Rekha, M.; Mahendra Perumal, G.; Shanmugaiah, V. Bioactive metabolites from

ethyl acetate extract of leaves of *Melia dubia* L., against human and plant microbial pathogens. *J. Adv. Microbiol. Res.* 2021, 2 (1), 13−21.

(11) Baek, M. Y.; Cho, J. G.; Lee, D. Y.; Ahn, E. M.; Jeong, T. S.; Baek, N. I. Isolation of triterpenoids from the stem bark of *Albizia julibrissin* and their inhibition activity on ACAT-1 and ACAT-2. *J. Korean Soc. Appl. Biol. Chem.* 2010, 53 (3), 310−315.

(12) Razdan, T. K.; Harkar, S.; Qadri, B.; Qurishi, M. A.; Khuroo, M. A. Lupene derivatives from *Skimmia laureola*. *Phytochemistry* 1988, 27 (6), 1890−1892.

(13) Miyazawa, M.; Uemura, T.; Kameoka, H. Biotransformation of sesquiterpenoids, (−)-globulol and (+)-ledol by *Glomerella cingulata*. *Phytochemistry* 1994, 37 (4), 1027−1030.

(14) Nguyen, V. B.; Wang, S. L.; Nguyen, T. H.; Nguyen, M. T.; Doan, C. T.; Tran, T. N.; Lin, Z. H.; Nguyen, Q. V.; Kuo, Y. H.; Nguyen, A. D. Novel potent hypoglycemic compounds from *Euonymus laxiflorus* Champ. and their effect on reducing plasma glucose in an ICR mouse model. *Molecules* 2018, 23 (8), 1928.

(15) Larsson, J.; Gottfries, J.; Muresan, S.; Backlund, A. ChemGPS-NP: tuned for navigation in biologically relevant chemical space. *J. Nat. Prod.* 2007, 70 (5), 789−794.

(16) Rosen, J.; Lovgren, A.; Kogej, T.; Muresan, S.; Gottfries, J.; Backlund, A. ChemGPS-NP$_{Web}$: chemical space navigation online. *J. Comput.-Aided Mol. Des.* 2009, 23 (4), 253−259.

(17) Tripathi, A.; Bankaitis, V. A. Molecular docking: from lock and key to combination lock. *J. Mol. Med. Clin. Appl.* 2017, 2, 1−9.

(18) Meng, X. Y.; Zhang, H. X.; Mezei, M.; Cui, M. Molecular docking: a powerful approach for structure-based drug discovery. *Curr. Comput. Aided Drug Des.* 2011, 7 (2), 146−157.

(19) Zeng, Q.; Guan, B.; Qin, J. J.; Wang, C. H.; Cheng, X. R.; Ren, J.; Yan, S. K.; Jin, H. Z.; Zhang, W. D. 2,3-Seco- and 3,4-seco-tirucallane triterpenoid derivatives from the stems of *Aphanamixis grandifolia* Blume. *Phytochemistry* 2012, 80, 148−155.

(20) Pandreka, A.; Chaya, P. S.; Kumar, A.; Aarthy, T.; Mulani, F. A.; Bhagyashree, D. D.; B, S. H.; Jennifer, C.; Ponnusamy, S.; Nagegowda, D.; Thulasiram, H. V. Limonoid biosynthesis 3: functional characterization of crucial genes involved in neem limonoid biosynthesis. *Phytochemistry* 2021, 184, 112669.

(21) Yang, S. C.; Chung, P. J.; Ho, C. M.; Kuo, C. Y.; Hung, M. F.; Huang, Y. T.; Chang, W. Y.; Chang, Y. W.; Chan, K. H.; Hwang, T. L. Propofol inhibits superoxide production, elastase release, and chemotaxis in formyl peptide-activated human neutrophils by blocking formyl peptide receptor 1. *J. Immunol.* 2013, 190 (12), 6511−6519.

(22) Brown, K. A.; Brain, S. D.; Pearson, J. D.; Edgeworth, J. D.; Lewis, S. M.; Treacher, D. F. Neutrophils in development of multiple organ failure in sepsis. *Lancet* 2006, 368 (9530), 157−169.

(23) Wu, S. F.; Chang, F. R.; Wang, S. Y.; Hwang, T. L.; Lee, C. L.; Chen, S. L.; Wu, C. C.; Wu, Y. C. Anti-inflammatory and cytotoxic neoflavonoids and benzofurans from *Pterocarpus santalinus*. *J. Nat. Prod.* 2011, 74 (5), 989−996.

(24) Sarigaputi, C.; Sangpech, N.; Palaga, T.; Pudhom, K. Suppression of inducible nitric oxide synthase pathway by 7-deacetylgedunin, a limonoid from *Xylocarpus* sp. *Planta Med.* 2015, 81 (04), 312−319.

(25) Garcin, E. D.; Arvai, A. S.; Rosenfeld, R. J.; Kroeger, M. D.; Crane, B. R.; Andersson, G.; Andrews, G.; Hamley, P. J.; Mallinder, P. R.; Nicholls, D. J.; St-Gallay, S. A.; Tinker, A. C.; Gensmantel, N. P.; Mete, A.; Cheshire, D. R.; Connolly, S.; Stuehr, D. J.; Aberg, A.; Wallace, A. V.; Tainer, J. A.; Getzoff, E. D. Anchored plasticity opens doors for selective inhibitor design in nitric oxide synthase. *Nat. Chem. Biol.* 2008, 4 (11), 700−707.

(26) Hu, H. C.; Yu, S. Y.; Hung, X. S.; Su, C. H.; Yang, Y. L.; Wei, C. K.; Cheng, Y. B.; Wu, Y. C.; Yen, C. H.; Hwang, T. L.; Chen, S. L.; Szatmari, I.; Hunyadi, A.; Tsai, Y. H.; Chang, F. R. Composition decipherment of *Ficus pumila* var. *awkeotsang* and its potential on COVID-19 symptom amelioration and *in silico* prediction of SARS-CoV-2 interference. *J. Food Drug Anal.* 2022, 30 (3), 440−453.

(27) Wu, G.; Robertson, D. H.; Brooks, C. L.; Vieth, M. Detailed analysis of grid-based molecular docking: a case study of CDOCKER-

A CHARMm-based MD docking algorithm. *J. Comput. Chem.* 2003, 24 (13), 1549−1562.

(28) da Silva, P. R.; do Espírito Santo, R. F.; Melo, C. D.; Pachú Cavalcante, F. E.; Costa, T. B.; Barbosa, Y. V.; e Silva, Y. M. S. d. M.; de Sousa, N. F.; Villarreal, C. F.; de Moura, R. O.; dos Santos, V. L. The compound (*E*)-2-Cyano-*N*,3-diphenylacrylamide (JMPR-01): a potential drug for treatment of inflammatory diseases. *Pharmaceutics* 2022, 14, 188.

(29) Buonfiglio, R.; Engkvist, O.; Varkonyi, P.; Henz, A.; Vikeved, E.; Backlund, A.; Kogej, T. Investigating pharmacological similarity by charting chemical space. *J. Chem. Inf. Model.* 2015, 55 (11), 2375−2390.

(30) Wilson, R. A.; Talbot, N. J. Under pressure: investigating the biology of plant infection by *Magnaporthe oryzae*. *Nat. Rev. Microbiol.* 2009, 7 (3), 185−195.

(31) Barchenger, D. W.; Lamour, K. H.; Bosland, P. W. Challenges and strategies for breeding resistance in *Capsicum annuum* to the multifarious pathogen, *Phytophthora capsici*. *Front. Plant Sci.* 2018, 9, 628.

(32) Khan, M. A.; Al Mamun Khan, M. A.; Mahfuz, A.; Sanjana, J. M.; Ahsan, A.; Gupta, D. R.; Hoque, M. N.; Islam, T. Highly potent natural fungicides identified in silico against the cereal killer fungus *Magnaporthe oryzae*. *Sci. Rep.* 2022, 12 (1), 20232.

(33) Eisenman, H. C.; Casadevall, A. Synthesis and assembly of fungal melanin. *Appl. Microbiol. Biotechnol.* 2012, 93 (3), 931−940.

(34) Liu, S.; Youngchim, S.; Zamith-Miranda, D.; Nosanchuk, J. D. Fungal melanin and the mammalian immune system. *J. Fungi* 2021, 7 (4), 264.

(35) Gomez, B. L.; Nosanchuk, J. D. Melanin and fungi. *Curr. Opin. Infect. Dis.* 2003, 16 (2), 91−96.

(36) Ikeda, R.; Sugita, T.; Jacobson, E. S.; Shinoda, T. Effects of melanin upon susceptibility of *Cryptococcus* to antifungals. *Microbiol. Immunol.* 2003, 47 (4), 271−277.

(37) Chen, H.; Han, X.; Qin, N.; Wei, L.; Yang, Y.; Rao, L.; Chi, B.; Feng, L.; Ren, Y.; Wan, J. Synthesis and biological evaluation of novel inhibitors against 1,3,8-trihydroxynaphthalene reductase from *Magnaporthe grisea*. *Bioorg. Med. Chem.* 2016, 24, 1225−1230.

(38) Chen, C. Y.; Liaw, C. C.; Chen, Y. H.; Chang, W. Y.; Chung, P. J.; Hwang, T. L. A novel immunomodulatory effect of ugonin U in human neutrophils via stimulation of phospholipase C. *Free Radical Biol. Med.* 2014, 72, 222−231.

(39) Gakuubi, M. M.; Maina, A. W.; Wagacha, J. M. Antifungal activity of essential oil of *Eucalyptus camaldulensis* Dehnh. against selected *Fusarium* spp. *Int. J. Microbiol.* 2017, 2017, 8761610.

(40) Purnomo, K. A.; Korinek, M.; Tsai, Y. H.; Hu, H. C.; Wang, Y. H.; Backlund, A.; Hwang, T. L.; Chen, B. H.; Wang, S. W.; Wu, C. C.; Chang, F. R. Decoding multiple biofunctions of maca on its anti-allergic, anti-inflammatory, anti-thrombotic, and pro-angiogenic activities. *J. Agric. Food Chem.* 2021, 69 (40), 11856−11866.

(41) Kowalski, M. L.; Asero, R.; Bavbek, S.; Blanca, M.; Blanca-Lopez, N.; Bochenek, G.; Brockow, K.; Campo, P.; Celik, G.; Cernadas, J.; Cortellini, G.; Gomes, E.; Nizankowska-Mogilnicka, E.; Romano, A.; Szczeklik, A.; Testi, S.; Torres, M. J.; Wohrl, S.; Makowska, J. Classification and practical approach to the diagnosis and management of hypersensitivity to nonsteroidal anti-inflammatory drugs. *Allergy* 2013, 68 (10), 1219−1232.

(42) Bindu, S.; Mazumder, S.; Bandyopadhyay, U. Non-steroidal anti-inflammatory drugs (NSAIDs) and organ damage: a current perspective. *Biochem. Pharmacol.* 2020, 180, 114147.

(43) Miura, T. Reactivity of nonsteroidal anti-inflammatory drugs with peroxidase: a classification of nonsteroidal anti-inflammatory drugs. *J. Pharm. Pharmacol.* 2012, 64 (10), 1461−1471.

(44) Zubrod, J. P.; Bundschuh, M.; Arts, G.; Bruhl, C. A.; Imfeld, G.; Knabel, A.; Payraudeau, S.; Rasmussen, J. J.; Rohr, J.; Scharmuller, A.; Smalling, K.; Stehle, S.; Schulz, R.; Schafer, R. B. Fungicides: an overlooked pesticide class? *Environ. Sci. Technol.* 2019, 53 (7), 3347−3365.

(45) Hollomon, D. W. Fungicide resistance: facing the challenge - a review. *Plant Protect. Sci.* 2015, 51 (4), 170−176.